

# Specular Reflection Image Enhancement Based on a Dark Channel Prior

Volume 13, Number 1, February 2021

Ye Xin  
Zhenhong Jia  
Jie Yang  
Nikola K. Kasabov, *Fellow, IEEE*



(a)



(b)

DOI: 10.1109/JPHOT.2021.3053906

# Specular Reflection Image Enhancement Based on a Dark Channel Prior

Ye Xin <sup>1,2</sup>, Zhenhong Jia <sup>1,2</sup>, Jie Yang <sup>3</sup>  
and Nikola K. Kasabov <sup>4,5</sup> *Fellow, IEEE*

<sup>1</sup>College of Information Science and Engineering, Xinjiang University, Urumqi 830046, China

<sup>2</sup>Key Laboratory of Signal Detection and Processing, Xinjiang Uygur Autonomous Region, Xinjiang University, Urumqi 830046, China

<sup>3</sup>Institute of Image Processing and Pattern Recognition, Shanghai Jiao Tong University, Shanghai 200400, China

<sup>4</sup>School of Engineering, Computing and Mathematical Sciences, Auckland University of Technology, Auckland 1020, New Zealand

<sup>5</sup>Intelligent Systems Research Center - Ulster University, Magee campus BT48 7JL, U.K.

DOI:10.1109/JPHOT.2021.3053906

This work is licensed under a Creative Commons Attribution 4.0 License. For more information, see <https://creativecommons.org/licenses/by/4.0/>

Manuscript received November 2, 2020; revised January 17, 2021; accepted January 20, 2021. Date of publication January 22, 2021; date of current version February 10, 2021. This work was supported in part by the National Science Foundation of China under Grant U1803261 and in part by the International Science and Technology Cooperation Project of the Ministry of Education of the People's Republic of China under Grant DICE 2016–2196. Corresponding author: Ye Xin (e-mail: xy1747259062@163.com).

**Abstract:** In this paper, we propose a specular highlight image enhancement algorithm based on a dark channel prior to solve the problem of information loss in specular highlight images in real scenes. First, the algorithm is based on the dark channel prior algorithm, and a moving window minimum filter is used to estimate the global illumination component. Then, a weighted function based on the local pixel color difference is introduced to solve the halo artifacts in the image. Then, the improved guided filter algorithm is used to optimize the transmittance, which improves the computational efficiency of the algorithm. Finally, the brightness of the image is adjusted by the CLAHE algorithm to enhance the local details of the image. Experimental results show that this method can effectively enhance the information in specular highlight images, and its processing results are obviously better than those of other algorithms.

**Index Terms:** Image enhancement, specular highlight image, dark channel prior, CLAHE, guided filtering.

## 1. Introduction

In the field of computer vision, most algorithms assume that the surface of an object is an ideal diffuse reflection surface, without considering the effect of specular reflection. In the real world, the specular reflection phenomenon is inevitable. The presence of highlights in the image will often cover the texture of the surface of the object, damage the contour of the edge of the object, change the color of the surface of the object, and directly lead to the loss of information in the local area of the object surface. The highlights in the image will not only affect the quality of the image but also greatly interfere with the application research of image tracking, scene analysis, scene reconstruction, etc. Therefore, it is particularly important to enhance the highlight area in the image. The existing methods are mainly for the highlight removal technology of specular images.

The methods are divided into two categories according to the number of images used: methods based on multiple images and methods based on single images.

Multiple image-based approaches. Nayar *et al.* [1] improved a polarization-based method by incorporating the neighboring diffuse color information. Lin [2] removed the highlights by treating the specular pixels as outliers and matching the remaining diffuse parts in other views. Lin and Shum [3] obtained photometric images from two images with different illumination positions and used linear basis functions to separate specular reflection components. However, because the light source is usually fixed, the use of this method is limited. Sato and Ikeuchi [4] employed a dichromatic model for separation by analyzing color signatures in many images captured with a moving light source. Barsky and Petrou [5] identified specular pixels according to the intensity distribution and separated the specular component by using the dichromatic reflection model. Although this kind of method can effectively separate the specular component, it is not suitable for general cases because of the need for multiple images.

Single image-based approaches. The method of Klinker *et al.* [6] performs clustering of all the pixels in the RGB color space to determine diffuse colors. Bajcsy *et al.* [7] used the hue-saturation-lightness color space instead of the RGB space. By regarding highlight removal as an interactive inpainting process, Tan *et al.* [8] recovered the diffuse colors of specular pixels under illumination constraints. Tan and Ikeuchi [9], [10] further proposed methods based on noise, chromaticity analysis and linear basis functions. Tan *et al.* [11] proposed making a specular-free image by setting the maximum chromaticity of each pixel to an arbitrary scalar value. Mallick *et al.* [12], [13] proposed an SUV color space which is a rotation of the RGB space, that separated the specular and diffuse components into an S channel and UV channels. This SUV space was further used for highlight removal by iteratively eroding the specular channel using either a single image or video sequence. Inpainting techniques that synthetically fill in the missing regions using neighboring patterns have also been applied to recover diffuse colors [14], [15]. Li *et al.* [16] used specialized domain knowledge to guide the removal of specular highlights in facial images. Shen and Cai [17] approximated the chromaticity of diffuse reflection by that of an specular-free (SF) image and adjusted the highlight level by enforcing smooth color transition between diffuse and specular regions. The literature [18], [19] proposed using filtering to remove highlights. The literature [20]–[22] used an SF image for pixel clustering and determined the specular component by solving the dichromatic least-squares system. Kim *et al.* [23] obtained an approximated specular-free image by applying the dark channel prior. Nguyen *et al.* [24] used tensor voting for the separation of reflection components. Akashi *et al.* [25] proposed a method based on sparse nonnegative matrix factorization (NMF) to separate reflection components, but this method may fail in the case of strong specular reflection or noise. Suo *et al.* [26] defined  $l_2$  chromaticity and used it to generate a specular-free image. Ren *et al.* [27] introduced the color lines constraint into the dichromatic reflection model and proposed a fast highlight removal method.

Although most of the current specular highlight removal algorithms have obtained some achievements, there are still the following problems. First, the current research only focuses on removing the highlight component from the image, and does not involve the information of recovering the highlight image. Moreover, it is required to take the specular highlight image in a specific scene (as shown in Fig. 1). Second, for specular highlight images in the real life scene, the existing algorithms cannot remove the highlight components in the image very well, and there are still some limitations in its popularization and practicability.

Based on the shortcomings in the current literature on specular highlights, we propose a specular highlight image enhancement algorithm using a dark channel prior. Our research work mainly includes the following content. First, an improved dark channel prior algorithm is proposed for the first time to enhance specular highlight images in real scenes. Second, a moving window minimum filter is used to estimate the global atmospheric light and introduce a weighting function based on the local pixel color difference in the boundary constraint. Third, an improved guided filtering algorithm is proposed to optimize the transmission and to use the CLAHE algorithm to further adjust the brightness of the image to enhance the local details of the image.

The remainder of this paper is organized as follows: Section 2 presents a specular highlight image enhancement algorithm using a dark channel prior. The experimental results are discussed in Section 3. At last, the conclusion is drawn in Section 4.

## 2. Proposed Methods

In this section, we propose a specular highlight image enhancement algorithm based on the dark channel prior. First, the algorithm is based on the dark channel prior algorithm, and we need to identify the haziest pixel in the input image and filter each color channel by a moving window minimum filter to estimate global atmospheric light  $A$ . Second, the weighted function based on the local pixel color difference is introduced into the boundary constraint to solve the halo artifacts in the image. Then, the improved guided filter algorithm is used to optimize the transmission. Finally, in LAB space (CIE Lab color model), the  $L$  component of the image is processed by the CLAHE algorithm, and the  $A, B$  components are adaptive. By adjusting the brightness and contrast of the image, the local details of the image are enhanced.

### 2.1 Obtaining Dark Channel Prior

The model that is widely used in computer vision and computer graphics to describe the formation of images is as follows [28]:

$$I(x) = J(x)t(x) + A(1 - t(x)) \quad (1)$$

where  $I(x)$  is the observed intensity,  $A$  is the global atmospheric light,  $t(x)$  is scene transmission, which is bounded in the interval  $0 \leq t(x) \leq 1$  and is always correlated with scene depth,  $J(x)$  is the scene radiance,  $M \leq J(x) \leq N$ , and  $M$  and  $N$  are two constant vectors related to a given image.

In the homogenous atmosphere, the transmission is expressed as:

$$t(x) = e^{-\mu d(x)} \quad (2)$$

where  $\mu$  is the scattering coefficient of the atmosphere. This indicates that the scene radiance is attenuated exponentially with the scene depth  $d(x)$ .

Equation (1) implies that in RGB color space, vectors  $I(x)$ ,  $J(x)$  and  $A$  lie in the same plane, and their endpoints are collinear. The transmission  $t(x)$  can also be represented as the ratio of two line segments:

$$t(x) = \frac{\|A - I(x)\|}{\|A - J(x)\|} = \frac{A^\tau - I^\tau(x)}{A^\tau - J^\tau(x)} \quad (3)$$

where  $\tau \in \{r, g, b\}$  is the color channel index.

The goal of the image formation model is to recover the scene radiance  $J(x)$  from  $I(x)$  based on (1). This requires us to estimate the transmission function  $t(x)$  and the global atmospheric light  $A$ . Once  $t(x)$  and  $A$  are estimated, the scenic radiance can be recovered by:

$$J(x) = \frac{I(x) - A}{t(x)} + A \quad (4)$$

The dark channel prior theory was first introduced by He *et al.* [29] using statistical principles, according to which there exist one or more color channels that have pixels whose intensity is very low or even closer to 0 due to the presence of shadows in most of the image's non-sky areas.

According to this theory, for any image  $J$ , its dark channel can be expressed as:

$$J^{dark}(x) = \min_{y \in \Gamma(x)} \left( \min_{\tau \in \{r, g, b\}} J^\tau(y) \right), J^{dark} \rightarrow 0 \quad (5)$$

where  $J^{dark}$  is a single color channel of image  $J$ ,  $\tau$  is the color space composed of three RGB channels, and  $\Gamma$  is a local area centered on  $(x, y)$ . Divide both sides of formula (1) by  $A^\tau$ , and take

the minimum value of the pixel blocks at both ends to get:

$$\min_{y \in \Gamma(x)} \left( \min_{\tau} \frac{I^{\tau}(x)}{A^{\tau}} \right) = \tilde{t}(x) \min_{y \in \Gamma(x)} \left( \min_{\tau} \frac{J^{\tau}(y)}{A^{\tau}} \right) + 1 - \tilde{t}(x) \quad (6)$$

where  $A^{\tau}$  is the image of the point with the strongest pixel intensity in the dark primary color image prime value. In the  $\Gamma(x)$  neighborhood,  $t(x)$  is a constant, denoted as  $\tilde{t}(x)$ . According to the dark primary color prior, the dark primary color channel  $J$  of the image after processing should tend to 0, and  $A$  is always a positive number, so it can be expressed as:

$$\min_{y \in \Gamma(x)} \left( \min_{\tau} \frac{J^{\tau}(y)}{A^{\tau}} \right) = 0 \quad (7)$$

Substituting (7) into (6), multiple parameters can be eliminated and the rough estimation expression of the radiation rate  $t(x)$  is:

$$\tilde{t}(x) = 1 - \alpha \min_{y \in \Gamma(x)} \left\{ \min_{\tau} \left[ \frac{I^{\tau}(x)}{A^{\tau}} \right] \right\} \quad (8)$$

where  $\alpha \in (0, 1]$  is the image fidelity adjustment factor.

To get  $J(x)$  it requires estimate of  $t(x)$  and  $A$  [30]. Once we know both  $t(x)$  and  $A$  then we can easily recover  $J(x)$  by:

$$J(x) = \frac{I(x) - A}{\max(t(x), t_0)} + A \quad (9)$$

where  $t_0$  is the lower limit of the transmittance set to avoid noise in the final processing results, usually the value is 0.1.

## 2.2 Estimation of the Global Atmospheric Light

In the dark channel prior algorithm, the gray value with the highest brightness is usually selected as the atmospheric light value. However, if there is a large area of high brightness area in the image, such as processing the specular highlight image, it is easy to cause the wrong estimation of atmospheric light  $A$ , resulting in color and distortion of the image; when the local area  $\Gamma(x)$  is in the position where the depth of field changes violently, the dark channel value will also be wrong, resulting in the halo effect of the processed image [30].

The global atmospheric light is used in the generation of transmission map and allow us to identify the color of atmospheric light. It is the multiplication of atmospheric luminance and the inverse of transmission map. Therefore, we propose an improved method for estimating global atmospheric light. Suppose that a part of the image contains pixels at infinity and treat the image points corresponding to pixels at infinity as a collection of representative color vectors of atmospheric brightness, and then apply an averaging operation to estimate the expected color vector of atmospheric brightness. In the input image, we pick up the brightest pixel which is the top 0.1% pixels according to the brightness of the image, and then a moving window minimum filter to filter each color channel, the maximum value of the color channel is taken as the estimated value of atmospheric light component  $A$ .

## 2.3 Weighted $l_1$ Norm Based Contextual Regularization

According to the theory that the depth value is constant in all pixels in a local image, we can use boundary constraints to deduce block-by-block transmission, but when the image depth changes suddenly, the image will have halo artifacts [31], [32]. Therefore, we construct the weighting function  $s(p, q)$  by calculating the color difference of local pixels on the boundary constraint, and the expression is:

$$s(p, q) (t(p) - t(q)) \approx 0 \quad (10)$$

where  $s(p, q)$  is the constraint between adjacent pixels  $p, q$  in the image.

If  $s(p, q) = 0$ , there is no constraint between adjacent pixels  $p, q$ , so it is particularly important to determine the value of  $s(p, q)$  [32].  $s(p, q)$  completely depends on the depth of the image. If the depth of the image between  $p$  and  $q$  is small, its value will be very large, so we can find  $t(x)$ ; in contrast, if the depth of the image between  $p$  and  $q$  is large, its value approaches 0. In this case, due to the lack of depth map information, we cannot construct  $t(x)$ .

Generally, the depth of an image varies with the intensity value between  $p$  and  $q$ , and pixels with the same intensity and color have similar depths [33]. Therefore, we construct the following weighting function based on this feature:

$$s(p, q) = e^{-\|I(p) - I(q)\|^2 / 2\gamma^2} \quad (11)$$

where  $\gamma$  is the specified parameter.

Then, we introduce the weighted context constraint into the image and calculate the regularization of  $t(x)$  as follows:

$$\int_{p \in \Phi} \int_{q \in \Phi} s(p, q) |t(p) - t(q)| dp dq \quad (12)$$

where  $\Phi$  is the image domain. By discretizing the above equation, we can obtain the following results:

$$\sum_{i \in I} \sum_{j \in s_i} s_{ij} |t_i - t_j| \quad (13)$$

By introducing a group of differential operators in (11), we can obtain:

$$\sum_{j \in s} \left\| S_j^o(L_j \otimes t) \right\| \quad (14)$$

where  $L_j$  is a first-order differential operator and  $S_j(j \in s)$  is a weighted matrix.

#### 2.4 Optimization of the Transmission

He *et al.* used a soft matting method to optimize the transmittance, but this method has high time complexity and a large amount of calculation, resulting in low efficiency of the algorithm. Therefore, this paper proposes an improved guided filtering algorithm to optimize the transmittance and improve the calculation efficiency of the algorithm.

The key to the guided filter is the local linear model between the guidance image  $I$  and the filtered image  $q$ . We assume that  $q$  is a linear transform of  $I$  in a window  $\omega_k$  centered at pixel  $k$ :

$$q_i = a_k I_i + b_k, \forall i \in \omega_k \quad (15)$$

where  $(a_k, b_k)$  are some linear coefficients assumed to be constant and  $\omega_k$  is a square window with a radius of  $r$ .

To minimize the difference between the input image  $p$  and the output image  $q$ , we define the cost function in the window  $\omega_k$  as:

$$E(a_k, b_k) = \min \sum_{i \in \omega_k} ((a_k I_i + b_k - p_i)^2 + \varepsilon \lambda a_k^2) \quad (16)$$

where  $\varepsilon$  is an adjustment parameter to prevent the value of  $a_k$  from being too large, and  $\lambda$  is the average value of the local variance in all pixels introduced into the cost function in the base layer to accurately maintain the edge of the image [34]. The expression is:

$$\lambda = \frac{1}{N} \sum_{k=1}^N \delta_k^2 \quad (17)$$

where  $\delta_k^2$  is the local variance in  $I$  in window  $\omega_k$ .

From the linear regression analysis, we can obtain the optimal values for  $(a_k, b_k)$ , as follows:

$$a_k = \frac{\frac{1}{|\omega|} \sum_{i \in \omega_k} l_i p_i - \mu_k \bar{p}_k}{\sigma_k^2 + \varepsilon \lambda} \quad (18)$$

$$b_k = \bar{p}_k - a_k \mu_k \quad (19)$$

where  $\delta_k^2$  and  $\mu_k$  are the variance and mean value in window  $\omega_k$ ,  $|\omega|$  is the number of pixels in window  $\omega_k$ , and

$\bar{p}_k = \frac{1}{|\omega|} \sum_{i \in \omega_k} p_i$ , is the mean value of  $p$  in the window.

Finally, the sliding window operation is adopted for the whole image, and the average value is obtained:

$$q_i = \frac{1}{|\omega|} \sum_{k: i \in \omega_k} (a_k l_i + b_k) = \bar{a}_i l_i + \bar{b}_i \quad (20)$$

where  $\bar{a}_k = \frac{1}{|\omega|} \sum_{k \in \omega_k} a_k$ ,  $\bar{b}_k = \frac{1}{|\omega|} \sum_{k \in \omega_k} b_k$ .

### 2.5 Brightness Enhancement

When the dark channel prior algorithm is used to process specular highlight images, there are large areas of high brightness areas in the image, which makes the processed image exhibit uneven brightness and low contrast. Therefore, we introduce the contrast limited adaptive histogram equalization algorithm (CLAHE) to adjust the brightness of the image and enhance the mirror by improving the local contrast of the image and the local details of the highlight image. First, the processed image is transformed from RGB space to lab color space, and the luminance component  $L$  of the image is extracted; then, the luminance component  $L$  is processed by the CLAHE algorithm, and the  $A$  and  $B$  components are adapted; finally, we update the brightness component  $L$  of the image and convert the processed image from lab space to RGB color space, which not only adjusts the brightness and contrast of the image but also effectively enhances the image.

## 3. Experiment and Results

To verify the validity of the algorithm proposed in this paper, the experimental images are all specular highlight images taken randomly in real-life scenes. This section evaluates the enhanced specular highlight image and compare it with the methods proposed by Yang [19], Shen *et al.* [22], Akashi *et al.* [26], Yamamoto *et al.* [20]. This section includes two parts: part A evaluates the enhanced specular highlight image subjectively, and part B compares the processing results of this paper and other algorithms objectively. To prove the effectiveness of the proposed method, all compared approaches were implemented in MATLAB 2018a on a PC with an Intel Core i7-10510U CPU @ 1.80 GB of memory running a Windows 10 operating system.

### 3.1 Subjective Evaluation

As shown in Figs. 2-6, the specular highlighted images after enhancement were evaluated subjectively, and representative algorithms, Yang [18], Shen *et al.* [21], Akashi *et al.* [25], Yamamoto *et al.* [19], were selected for comparison with the algorithms proposed in this study. By observing the experimental image, it can be found that the presence of highlights in the original image makes some areas of the image very bright, which not only obstructs the information of the partial areas of the image but also changes the color of the image surface.

As shown in Fig. 2(b)–(e)–Fig. 6(b)–(e), the specular highlight image processed by references [18], [21], [25] and [19] does not recover the information of the local area blocked by the highlight in the image and loses the information of the non-highlight area of the image. The main reason



Fig. 1. The images involved in the existing specular reflection removal algorithm.

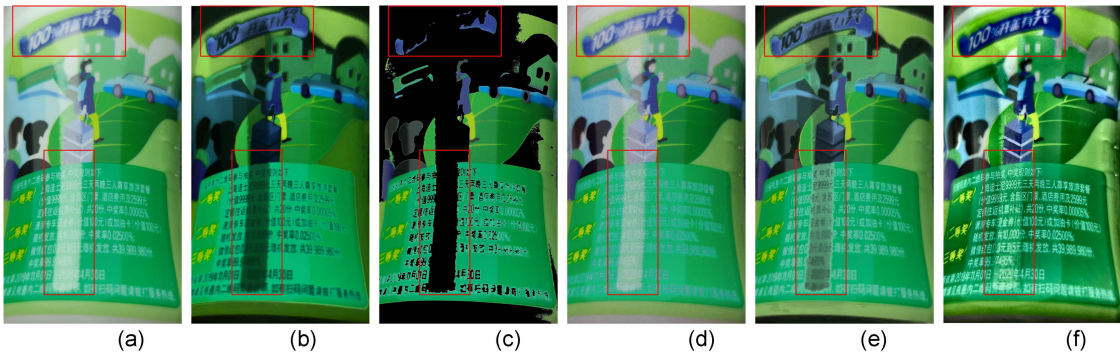


Fig. 2. (a) Original image, (b) Yang [18], (c) Shen *et al.* [21], (d) Akashi *et al.* [25], (e) Yamamoto *et al.* [20], (f) the proposed method.

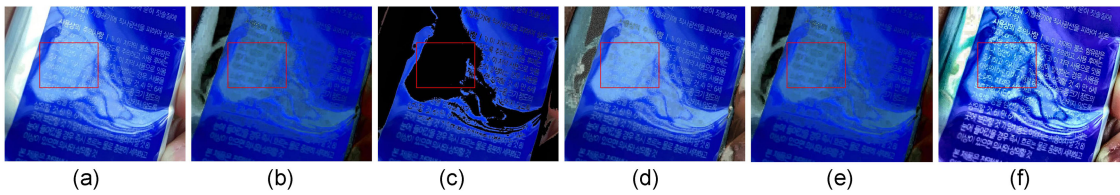


Fig. 3. (a) Original image, (b) Yang [18], (c) Shen *et al.* [21], (d) Akashi *et al.* [25], (e) Yamamoto *et al.* [20], (f) the proposed method.

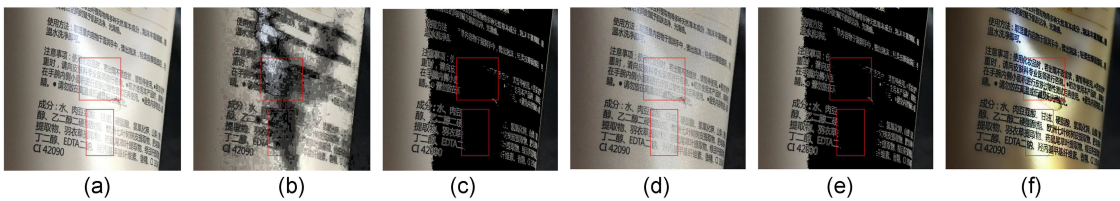


Fig. 4. (a) Original image, (b) Yang [18], (c) Shen *et al.* [21], (d) Akashi *et al.* [25], (e) Yamamoto *et al.* [20], (f) the proposed method.

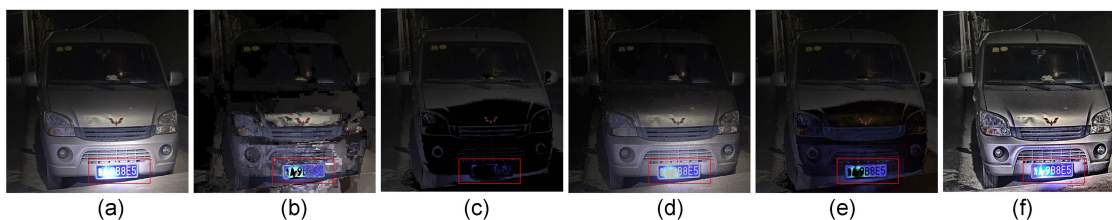


Fig. 5. (a) Original image, (b) Yang [18], (c) Shen *et al.* [21], (d) Akashi *et al.* [25], (e) Yamamoto *et al.* [20], (f) the proposed method.

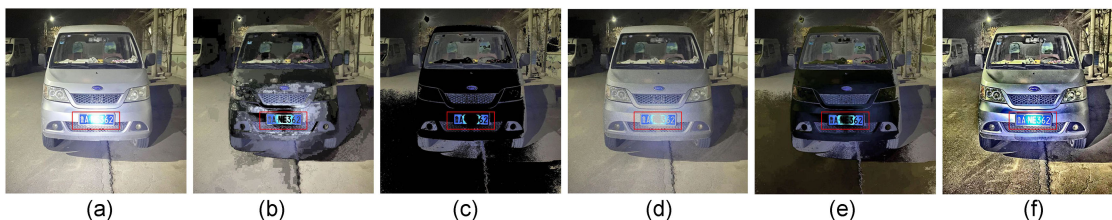


Fig. 6. (a) Original image, (b) Yang [18], (c) Shen *et al.* [21], (d) Akashi *et al.* [25], (e) Yamamoto *et al.* [20], (f) the proposed method.

for the above problems is that the above algorithm has certain constraints when processing specular highlight images and requires application in specific objects and scenes; in the process of image processing, the highlight components are mainly separated by estimating non-highlight components. The inaccuracy of the non-highlight component causes the problem of information loss when the image separates the highlight component. Therefore, the above algorithm cannot achieve satisfactory results when processing real specular highlight images. Compared with the algorithms in [18], [21], [25] and [19], the method proposed in this paper can recover the information of the highlight area in the image very well, as shown in the figure. As shown in Fig. 2(f)–Fig. 6(f), the image processed by the algorithm proposed in this paper retains more detailed features than the original image. The information of the highlighted area in the image is clearly visible and compared with other algorithms, the processed image effect is more obvious.

### 3.2 Objective Evaluation of Results

It is a very difficult task to objectively evaluate the enhanced specular highlight image because there are no real and reliable no-highlight images as a reference, so we use nonreference methods to analyze the processed results. To test the effect of each algorithm more comprehensively, we choose  $e$ ,  $r$ ,  $H$ ,  $\theta$  and  $CNI$  as evaluation indicators to compare the algorithms quantitatively, and we performed a qualitative no-reference quality assessment with 200 specular reflection images

The  $e$  measure represents the rate of newly visible edges after processing the image:

$$e = \exp \left( \frac{1}{v_e} \sum_{p_i \in \vartheta_e} \log e_i \right) \quad (21)$$

where  $e$  is the gradient ratio between the original image and the processed image, and  $\vartheta_e$  consists of the visible edges of the processed image [36].

Ratio of average gradient  $r$  represents the measure of enhancement contrast between the background and target by applying the technique,  $H$  and  $\theta$  are expressed as the information entropy and edge intensity, respectively.

TABLE I  
Highlight Images of FIGS. 2-6 Enhancement Evaluation Based on the  $e$  Metric. A Larger Metric is Better

|         | Original | Yang [19] | Shen et al. [22] | Akashi et al [26] | Yamamoto et al [20] | Our method |
|---------|----------|-----------|------------------|-------------------|---------------------|------------|
| Fig.2   | ---      | 0.685     | 1.417            | 3.236             | 1.195               | 2.378      |
| Fig.3   | ---      | 0.624     | 1.069            | 1.308             | 1.080               | 2.541      |
| Fig.4   | ---      | 2.758     | 1.271            | 3.254             | 1.268               | 1.328      |
| Fig.5   | ---      | 1.781     | 1.148            | 1.854             | 1.111               | 3.664      |
| Fig.6   | ---      | 1.693     | 1.328            | 2.099             | 1.156               | 4.090      |
| Average | ---      | 1.508     | 1.246            | 2.350             | 1.162               | 2.800      |

TABLE II  
Highlight Image of FIGS. 2-6 Enhancement Evaluation Based on the  $r$  Metric. A Larger Metric is Better

|         | Original | Yang [19] | Shen et al. [22] | Akashi et al [26] | Yamamoto et al [20] | Our method |
|---------|----------|-----------|------------------|-------------------|---------------------|------------|
| Fig.2   | 1.351    | 1.001     | 2.476            | 7.511             | 1.501               | 3.645      |
| Fig.3   | 3.477    | 1.470     | 4.283            | 4.706             | 3.645               | 7.609      |
| Fig.4   | 4.459    | 4.632     | 5.691            | 10.411            | 5.663               | 6.505      |
| Fig.5   | 2.462    | 2.477     | 1.753            | 4.249             | 1.932               | 4.259      |
| Fig.6   | 3.976    | 3.443     | 4.810            | 6.647             | 4.268               | 9.963      |
| Average | 3.145    | 2.604     | 3.802            | 6.704             | 3.401               | 6.396      |

TABLE III  
Highlight Image of FIGS. 2-6 Enhancement Evaluation Based on the  $H$  Metric. A Larger Metric is Better

|         | Original | Yang [19] | Shen et al. [22] | Akashi et al [26] | Yamamoto et al [20] | Our method |
|---------|----------|-----------|------------------|-------------------|---------------------|------------|
| Fig.2   | 7.650    | 7.338     | 5.118            | 7.686             | 7.543               | 7.691      |
| Fig.3   | 7.696    | 7.319     | 5.628            | 7.798             | 7.603               | 7.595      |
| Fig.4   | 7.715    | 7.708     | 4.720            | 7.713             | 4.713               | 7.719      |
| Fig.5   | 6.930    | 6.008     | 4.990            | 6.599             | 5.655               | 7.269      |
| Fig.6   | 7.586    | 7.584     | 5.029            | 7.656             | 7.004               | 7.875      |
| Average | 7.515    | 7.191     | 5.097            | 7.490             | 6.503               | 7.629      |

TABLE IV  
Highlight Images of FIGS. 2-6 Enhancement Evaluation Based on the  $\theta$  Metric. A Larger Metric is Better

|         | Original | Yang [19] | Shen et al. [22] | Akashi et al [26] | Yamamoto et al [20] | Our method |
|---------|----------|-----------|------------------|-------------------|---------------------|------------|
| Fig.2   | 14.401   | 10.891    | 24.173           | 53.633            | 15.865              | 39.735     |
| Fig.3   | 37.070   | 15.717    | 42.837           | 44.331            | 38.117              | 85.479     |
| Fig.4   | 47.735   | 47.785    | 54.554           | 82.033            | 54.298              | 67.662     |
| Fig.5   | 26.213   | 26.172    | 17.021           | 35.703            | 19.250              | 76.206     |
| Fig.6   | 60.331   | 36.163    | 45.632           | 70.283            | 40.260              | 148.546    |
| Average | 37.150   | 27.345    | 36.843           | 57.166            | 33.558              | 83.526     |

The percentage of pixels which becomes completely black or white in the enhanced image and Colour Naturalness Index ( $CNI$ ), higher value of  $CNI$  indicates the enhanced image is more natural [37].

Tables I–VI summarize the results of random specular highlight image processing in different real scenes by using Yang [18], Shen *et al.* [21], Akashi *et al.* [25], Yamamoto *et al.* [19] and the algorithm proposed in this study. It can be seen from Table V that in the processing effect of a few pictures, the value of our  $CNI$  is not as good as other algorithms, but the gap is not very large. Generally speaking, compared with other algorithms, our algorithm has more advantages, indicating that the image processed by this method is more natural. In Table VI, we select 200 specular highlight images in different scenes and compare the results of the above algorithms. By analyzing the above data, we find that using  $e$ ,  $r$ ,  $H$ ,  $\theta$  and  $CNI$  as the measurement method, the indexes of this algorithm

TABLE V  
Highlight Images of FIGS. 2-6 Enhancement Evaluation Based on the *CNI* Metric. A Larger Metric is Better

|         | Original | Yang [19] | Shen et al. [22] | Akashi et al [26] | Yamamoto et al [20] | Our method |
|---------|----------|-----------|------------------|-------------------|---------------------|------------|
| Fig.2   | 0.834    | 0.836     | 0.593            | 0.889             | 0.571               | 0.716      |
| Fig.3   | 0.169    | 0.542     | 0.503            | 0.239             | 0.768               | 0.902      |
| Fig.4   | 0.468    | 0.552     | 0.633            | 0.541             | 0.524               | 0.563      |
| Fig.5   | 0.660    | 0.243     | 0.233            | 0.647             | 0.471               | 0.662      |
| Fig.6   | 0.530    | 0.464     | 0.468            | 0.144             | 0.566               | 0.741      |
| Average | 0.532    | 0.527     | 0.486            | 0.492             | 0.580               | 0.717      |

TABLE VI  
Comparison of Average Enhancement Acquired by  $e$ ,  $r$ ,  $H$ ,  $\theta$  and *CNI* for 200 Specular Highlight Images

|            | Original | Yang [19] | Shen et al. [22] | Akashi et al [26] | Yamamoto et al [20] | Our method |
|------------|----------|-----------|------------------|-------------------|---------------------|------------|
| $e$        | --       | 1.001     | 1.081            | 1.653             | 1.015               | 3.331      |
| $r$        | 6.369    | 1.533     | 2.635            | 5.232             | 2.262               | 6.540      |
| $H$        | 7.288    | 6.788     | 5.145            | 7.213             | 6.634               | 7.607      |
| $\theta$   | 25.794   | 23.483    | 28.110           | 44.455            | 24.310              | 102.31     |
| <i>CNI</i> | 0.425    | 0.532     | 0.358            | 0.529             | 0.478               | 0.625      |

are mostly higher than other algorithms, which shows that the algorithm in this paper has better performance than other algorithms in enhancing specular highlight images. The edge contrast, clarity and detail features of the image processed by this algorithm are obviously enhanced, and the local information of the specular highlight image is effectively restored. Therefore, through the comprehensive comparison of the enhancement effect of specular highlight images in different scenes, it can be concluded that the effectiveness of the proposed algorithm is better than that of the other algorithms.

#### 4. Conclusion

In this study, we focus on the images affected by highlights in real-life scenes. Our purpose is to enhance the information in specular highlight images so that the images are clearer, easier to identify and more valuable for practical application. Therefore, we propose a specular highlight image enhancement algorithm based on the dark channel prior. First, the algorithm is based on the dark channel prior and effectively estimates the global illumination component of the image by a moving window filter. Then, the weighting function based on the local pixel chromatic aberration is introduced in the boundary constraint to solve the existence of the image and the problem of halo artifacts. Next, the improved guided filter algorithm is used to optimize the transmittance and increase the calculation efficiency of the algorithm. Finally, in the LAB space, the CLAHE algorithm is used to enhance the image's brightness component  $L$ ,  $A$ ,  $B$  which is adaptive through adjusting the contrast of the image and enhancing the local details of the image. Experimental results show that the algorithm proposed in this study is significantly better than other algorithms based on both subjective and objective evaluations. Further research is anticipated towards specular highlight image enhancement of images from moving objects. A potential approach would be the use of spiking neural networks and dynamic vision sensors [35].

#### References

- [1] S. K. Nayar, X. Fang, and T. E. Boult, "Separation of reflection components using color and polarization," *Int. J. Comput. Vis.*, vol. 21, pp. 163–186, 1997.
- [2] S. Lin, Y. Li, S. B. Kang, X. Tong, and H. Shum, "Diffuse-specular separation and depth recovery from image sequences," in *Proc. Eur. Conf. Comput. Vis.*, 2002, pp. 210–224.

- [3] S. Lin and H. Y. Shum, "Separation of diffuse and specular reflection in color images," in *Proc. IEEE Comput. Soc. Conf. Comput. Vis. Pattern Recognit.*, 2003, p. 1.
- [4] Y. Sato and K. Ikeuchi, "Temporal-color space analysis of reflection," *J. Opt. Soc. Amer. A.*, vol. 11, pp. 2990–3002, 1994.
- [5] S. Barsky and M. Petrou, "The 4-source photometric stereo technique for three-dimensional surfaces in the presence of highlights and shadows," *IEEE Trans. Pattern Anal. Mach. Intell.*, vol. 25, no. 10, pp. 1239–1252, Oct. 2003.
- [6] G. Klinker, S. A. Shafer, and T. Kanade, "The measurement of highlights in color images," *Int. J. Comput. Vis.*, vol. 2, pp. 309–334, 1992.
- [7] R. Bajcsy, W. L. Sang, and A. Leonardis, "Detection of diffuse and specular interface reflections and inter-reflections by color image segmentation," *Int. J. Comput. Vis.*, vol. 17, pp. 241–272, 1996.
- [8] L. Pingtan, L. Quan, and H. Shum, "Highlight removal by illumination-constrained inpainting," in *Proc. Int. Conf. Comput. Vis.*, 2003, pp. 164–169.
- [9] R. T. Tan, K. Nishino, and K. Ikeuchi, "Separating reflection components based on chromaticity and noise analysis," *IEEE Trans. Pattern Anal. Mach. Intell.*, vol. 26, no. 10, pp. 1373–1379, Oct. 2004.
- [10] R. T. Tan and K. Ikeuchi, "Reflection components decomposition of textured surfaces using linear basis functions," in *Proc. Comput. Vis. Pattern Recognit.*, 2005, pp. 125–131.
- [11] R. T. Tan and K. Ikeuchi, "Separating reflection components of textured surfaces using a single image," *IEEE Trans. Pattern Anal. Mach. Intell.*, vol. 27, no. 2, pp. 178–193, Feb. 2005.
- [12] S. P. Mallick, T. Zickler, D. J. Kriegman, and P. N. Belhumeur, "Beyond lambert: Reconstructing specular surfaces using color," in *Proc. Comput. Vis. Pattern Recognit.*, 2005, pp. 619–626.
- [13] S. P. Mallick, T. Zickler, P. N. Belhumeur, and D. J. Kriegman, "Specularity removal in images and videos: A PDE approach," *Comput. Vis.—ECCV*, vol. 3951, pp. 550–563, 2006.
- [14] L. Pingtan, L. Quan, and H. Shum, "Highlight removal by illumination-constrained inpainting," in *Proc. Int. Conf. Comput. Vis.*, 2003, pp. 164–169.
- [15] P. Tan, L. Quan, and S. Lin, "Separation of highlight reflections on textured surfaces," in *Proc. IEEE Comput. Soc. Conf. Comput. Vis. Pattern Recognit.*, 2006, pp. 1855–1860.
- [16] L. Chen, S. Lin, K. Zhou, and K. Ikeuchi, "Specular highlight removal in facial images," in *Proc. IEEE Conf. Comput. Vis. Pattern Recognit.*, 2017, pp. 2780–2789.
- [17] H. L. Shen and Q. Y. Cai, "Simple and efficient method for specularity removal in an image," *Appl. Opt.*, vol. 48, pp. 2711–2719, 2009.
- [18] Q. Yang, S. Wang, and N. Ahuja, "Real-time specular highlight removal using bilateral filtering," *Comput. Vis.—ECCV*, vol. 6314, pp. 87–100, 2010.
- [19] T. Yamamoto and A. Nakazawa, "General improvement method of specular component separation using high-emphasis filter and similarity function," *ITE Trans. Media Technol. Appl.*, vol. 7, pp. 92–102, 2019.
- [20] H. L. Shen, H. G. Zhang, S. J. Shao, and J. H. Xin, "Chromaticity-based separation of reflection components in a single image," *Pattern Recognit.*, vol. 41, pp. 2461–2469, 2008.
- [21] H. Shen and Z. Zheng, "Real-time highlight removal using intensity ratio," *Appl. Opt.*, vol. 52, pp. 4483–4493, 2013.
- [22] Y. Liu, Z. Yuan, N. Zheng, and Y. Wu, "Saturation-preserving specular reflection separation," in *Proc. IEEE Conf. Comput. Vis. Pattern Recognit.*, 2015, pp. 3725–3733.
- [23] H. Kim, H. Jin, S. Hadap, and I. Kweon, "Specular reflection separation using dark channel prior," in *Proc. Comput. Vis. Pattern Recognit.*, 2013.
- [24] T. Nguyen, Q. N. Vo, H. J. Yang, S. H. Kim, and G. S. Lee, "Separation of specular and diffuse components using tensor voting in color images," *Appl. Opt.*, vol. 53, pp. 7924–7936, 2014.
- [25] Q. Yang, S. Wang, and N. Ahuja, "Real-time specular highlight removal using bilateral filtering," *Comput. Vis.*, 2011, pp. 87–100.
- [26] J. Suo, D. An, X. Ji, H. Wang, and Q. Dai, "Fast and high quality highlight removal from a single image," *IEEE Trans. Image Process.*, vol. 25, no. 11, pp. 5441–5454, Nov. 2016.
- [27] W. Ren, J. Tian, and Y. Tang, "Specular reflection separation with color-lines constraint," *IEEE Trans. Image Process.*, vol. 26, no. 5, pp. 2327–2337, May 2017.
- [28] E. J. McCartney and F. F. Hall, "Optics of the atmosphere: Scattering by molecules and particles," *Phys. Today*, vol. 30, pp. 76–77, 1977.
- [29] K. He, J. Sun, and X. Tang, "Single image haze removal using dark channel prior," in *Proc. Comput. Vis. Pattern Recognit.*, 2009, pp. 1956–1963.
- [30] G. Meng, Y. Wang, J. Duan, S. Xiang, and C. Pan, "Efficient image dehazing with boundary constraint and contextual regularization," in *Proc. IEEE Int. Conf. Comput. Vis.*, 2013, pp. 617–624.
- [31] V. Khanadelwal, D. Mangal, and N. Kumar, "Elimination of fog in single image using dark-channel prior," *Int. Res. J. Eng. Technol.*, vol. 5, pp. 1602–1609, 2018.
- [32] W. Kumar and S. S. Urmila, "Single image dehazing for robust image matching," *Int. J. Adv. Res. Comput. Commun. Eng.*, vol. 5, pp. 13–19, 2016.
- [33] N. Kumar and S. Manjunath, "Efficient single image defogging using radiance cube an L norm based regularization matching," *Int. J. Technol. Res. Eng.*, vol. 2, pp. 1778–1780, 2015.
- [34] Z. Lu, B. Long, K. Li, and F. Lu, "Effective guided image filtering for contrast enhancement," *IEEE Signal Process. Lett.*, vol. 25, no. 10, pp. 1585–1589, Oct. 2018.
- [35] N. K. Kasabov, "Time-space spiking neural networks and brain-inspired artificial intelligence," *Evolv. Spik. Neural Netw.*, Springer, vol. 7, pp. 169–199, 2018.
- [36] I. Kansal and S. S. Kasana, "Minimum preserving subsampling-based fast image de-fogging," *J. Modern Opt.*, vol. 65, no. 18, pp. 2103–2123, 2018.
- [37] I. Kansal and S. S. Kasana, "Improved color attenuation prior based image de-fogging technique," *Multimedia Tools Appl.*, vol. 79, no. 11, 2020.